J Appl Electrochem (2008) 38:751–758
DOI 10.1007/s10800-008-9504-8

ORIGINAL PAPER

Electrochemical behaviour of a new triiron-substituted polyoxomolybdate

Graziella Liana Turdean · Adrian Patrut · Leontin David · Ionel Catalin Popescu

Received: 17 October 2007 / Revised: 18 January 2008 / Accepted: 28 January 2008 / Published online: 13 February 2008

Abstract A new complex of the Keggin trilacunary $A\alpha$-$PMo_9O_{34}^{9-}$ polyoxomolybdate (PMo_9) with Fe^{3+} ions, having the formula $A\alpha$-$PFe_3^{III}(H_2O)_3Mo_9O_{37}^{6-}$ (PFe_3Mo_9), has been synthesized and characterized by chemical analysis, FT-IR, Raman, UV-VIS-NIR and EPR spectroscopy, as well as by magnetic susceptibility measurements. Cyclic voltammetry performed at different scan rates, pH and supporting electrolyte composition, was used to investigate the electrochemical behaviour of the PFe_3Mo_9 complex in acidic medium and its electrocatalytic effect on H_2O_2 reduction. The voltammetric waves were assigned, and the enhanced electrocatalytic efficiency of PFe_3Mo_9 relative to PMo_9 was attributed to the presence of Fe atoms.

Keywords Polyoxomolybdate · Keggin structure · Iron complex · Cyclic voltammetry · Hydrogen peroxide electroreduction

1 Introduction

Polyoxometalates, also called metal-oxygen clusters, are the most important representatives of the inorganic molecular nanoclusters. The continuous diversification of polyoxometalates through the synthesis of an impressive number of new substances, with interesting electronic structures, high symmetry, unexpected topologies, various electron-transfer processes and remarkable magnetic-exchange interactions has led to many applications, especially in catalysis, analysis, medicine, biochemistry and materials science [1–7].

Lacunary polyoxometalates are synthesized, or at least formally derived, from their complete precursor structure, by removing one or several addenda atoms. They act as ligands and exhibit an increased reactivity towards transition and inner transition metals, thus forming a broad variety of complexes with different stoichiometry [8–10]. Complexes of lacunary polyoxometalates with lower-valent transition metals exhibit surfaces analogous to those of close-packed metal oxide lattices, yielding a soluble model of an oxide surface [11–13]. Such complexes have attracted considerable interest owing to their ability to replace metalloporphyrins and other metal complexes of macrocyclic ligands as catalysts in many reactions [14–16]. Consequently, many complexes of lacunary polyoxometalates with transition metals have been prepared and their catalytic activity was investigated. Usually, the incorporated transition metal centre(s) is (are) the active site(s) for electrocatalysis. Therefore, the electrochemical investigation of the incorporated metal centre(s) is very important in order to design the electrocatalyst for one particular reaction. These complexes are also interesting in regard to the mechanisms of the electron-transfer reactions in which they are engaged [17–19].

Out of the large variety of complexes of lacunary polyoxometalates with transition metals, attention was paid to the electrochemical behaviour and properties of two different types: (i) mono-, di- and trimetal complexes of the

G. L. Turdean · I. C. Popescu (✉)
Department of Physical Chemistry, Babeş-Bolyai University, 11 Arany Janos, 400028 Cluj-Napoca, Romania
e-mail: cpopescu@chem.ubbcluj.ro

A. Patrut
Department of Inorganic Chemistry, Babeş-Bolyai University, 11 Arany Janos, 400028 Cluj-Napoca, Romania

L. David
Department of Physics, Babeş-Bolyai University, 1 M. Kogalniceanu, 400084 Cluj-Napoca, Romania

mono-, di- and trilacunary Keggin and Dawson polyoxometalates (so-called transition metal-substituted polyoxometalates) and (ii) sandwich-type complexes, with three or four transition metal centres coordinated by two trilacunary Keggin or Dawson polyoxometalates. Among them, the complexes with iron(III) have probably been the most studied [13, 17, 20–39].

Iron(III)-trisubstituted Keggin polyoxotungstates (M = W) have been synthesized and electrochemically investigated [13, 26]. However, trilacunary Keggin polyoxomolybdates (M=Mo) and especially their complexes have been much less studied, as they are more difficult to prepare and have lower stability. The trivacant $A\alpha$-$PMo_9O_{34}^{9-}$ phospho(V)polyoxomolybdate is derived from the parent α-$PMo_{12}O_{40}^{3-}$ Keggin structure, by removal of three adjacent Mo addenda from three different Mo_3O_{13} units [40].

A new complex of the trilacunary $A\alpha$-$PMo_9O_{34}^{9-}$ Keggin polyoxomolybdate (abbreviated as PMo_9) with Fe^{3+} ions was synthesized. The complex corresponds to the $A\alpha$-$PFe_3^{III}(H_2O)_3Mo_9O_{37}^{6-}$ formula and was abbreviated as PFe_3Mo_9. The triiron(III)-substituted phospho(V)polyoxomolybdate was characterized by chemical analysis, FT-IR, Raman, UV-VIS-NIR and electron paramagnetic resonance (EPR) spectroscopy, as well as by magnetic susceptibility measurements.

In this paper, we also report the main results of cyclic voltammetry (CV) performed on the PFe_3Mo_9 complex, in acidic medium. The electrocatalytic effect of this complex on the reduction of H_2O_2 was addressed. CV was carried out under various experimental conditions, namely, at different scan rates, pH and composition of the supporting electrolyte. Our findings make it possible to assign the reduction/oxidation peaks retrieved in CV, and support the beneficial effect of the presence of Fe atoms on the electrocatalytic activity of the PFe_3Mo_9 complex for H_2O_2 reduction.

2 Experimental

2.1 Methods

Elemental analysis of P, Mo and Fe was performed by OES-ICP with a BIRD 2070 spectrophotometer. Na was determined by FEP using an Eppendorf flame photometer. Water content was measured by dehydration at 350 °C.

Vibrational spectra were recorded in the 4,000–400 cm^{-1} range on a Bruker FTIR IFS 66 with a Raman FRA 106 unit spectrophotometer (λ_e = 1,064 nm), using KBr pellets. Electronic spectra in aqueous solution were acquired in the 190–1,000 nm range with an ATI Unicam-UV-Visible spectrophotometer, by means of a Vision Software V 3.20. The EPR spectrum was recorded on powdered solids, at room temperature, in the X-band (9.56 GHz) using a Bruker ESP 380 spectrometer. Magnetic susceptibility measurements were carried out with a Faraday type balance in the 77–290 K temperature range.

CV measurements were performed in a conventional electrochemical cell, using a computer controlled voltammetric analyzer (Autolab-PGSTAT 10, EcoChemie, Netherlands). The potential of the working electrode (graphite, ϕ = 2.5 mm; Ringsdorff, Bonn-Bad, Godesberg, Germany) was recorded against a Ag/AgCl, KCl_{sat} reference electrode (Radiometer, France). A platinum plate (S = 1 cm^2) served as counter electrode. Before each experiment, the working electrode was cleaned and polished using emery paper (600 grid). All electrochemical experiments were performed at room temperature and without prior degassing of the investigated solution.

2.2 Materials

The polyoxometalate solutions were freshly prepared just prior to use, by dissolving the appropriate amounts of salt in 0.5 M aqueous K_2SO_4 (Fluka) supporting electrolyte. The pH of the supporting electrolyte was adjusted with diluted H_2SO_4 in the pH range 1.5–3.5 and with 0.06 M phosphate buffer in the pH range 3.5–7. The 0.06 M phosphate buffer (pH 7) was prepared by mixing the appropriate volumes of $Na_2HPO_4 \cdot 12H_2O$ (Sigma) and KH_2PO_4 (Sigma) solutions. Hydrogen peroxide (30%) was provided by Silal Trading, Romania.

All chemicals were of analytical reagent grade. All syntheses and analytical investigations were carried out in distilled water.

2.3 Synthesis

The trilacunary $Na_3[A\alpha$-$H_6PMo_9O_{34}] \cdot 13H_2O$ polyoxometalate ligand was prepared according to the procedure described elsewhere [40]. Ten millilitres of an aqueous solution containing 2.42 g $Fe(NO_3)_3 \cdot 9H_2O$ (6 mmol) was added at 70 °C, under stirring, to a 20 mL aqueous solution containing 3.50 g ligand (2 mmol). The mixture was subsequently stirred for 3 h. After two weeks, deep green microcrystals of the $Na_3H_3[A\alpha$-$PFe_3^{III}(H_2O)_3Mo_9O_{37}] \cdot 14$ H_2O neutral complex precipitated and were collected by filtration, washed with NaCl solution (2 M), ethanol and ether and then recrystallized from hot water. Yield: 2.52 g (60.4% based on Fe).

The reaction of preparation can be written formally as:

$$A\alpha\text{-}PMo_9O_{34}^{9-} + 3FeO^{+} + 3H_2O \rightarrow A\alpha\text{-}PFe_3^{III}(H_2O)_3Mo_9O_{37}^{6-} \quad (1)$$

Elemental analysis of $H_{37}Na_3PFe_3Mo_9O_{54}$ (M = 2032.15), found (calculated): Na 3.47 (3.39), P 1.56

(1.52), Fe 8.04 (8.24), Mo 42.83 (42.49), H_2O 12.60 (12.41).

FT-IR (KBr pellet; polyoxometalate region, cm^{-1}): 1070 (s), 1036 (s), 962 (s), 902 (s), 858 (s), 781 (vs), 752 (s), 616 (m), 520 (m).

Raman (KBr pellet; cm^{-1}): 1002 (vs), 980 (m), 891 (w), 860 (w), 595 (m), 470 (m).

UV-VIS-NIR (nm): 208, 255 (sh), 280 (sh), 850.

3 Results and discussion

3.1 Spectroscopic and magnetic investigation

3.1.1 Vibrational spectra

Generally, IR and Raman spectra of polyoxometalates exhibit contributions of the polyoxometalate framework [41]. The main vibration due to the heteroatom, ν_{as}(P–O), which is observed only in the FT-IR spectrum, is recorded at 1,070 and 1,036 cm^{-1}. Its splitting in the PFe_3Mo_9 complex is smaller than in the PMo_9 ligand, i.e. 34 vs. 52 cm^{-1}. This indicates that the coordination of the three Fe^{3+} ions partially restores the tetrahedral symmetry of the PO_4 heterogroup and of the entire polyoxometalate anion, previously affected by the triple vacancy of the ligand. The ν_{as}(Mo=O) vibration, characteristic to polyoxomolybdates, is registered at 962 cm^{-1} in the FT-IR spectrum and 980 cm^{-1} in the Raman spectrum. The very intense ν_s(Mo=O) vibration, which is only Raman active, is recorded at 1,002 cm^{-1}. The ν(Mo–O–Mo) vibrations, also specific to the polyoxomolybdate structure, are observed in the 700–900 cm^{-1} range.

3.1.2 Electronic spectra

The UV spectrum of the PFe_3Mo_9 complex exhibits the two charge-transfer bands characteristic to the polyoxometalate structure [42]. The ν_2 band (208 nm) is due to dπ–pπ transitions of the $Mo{=}O_t$ bonds. Its molar absorptivity is proportional to the number of Mo atoms and has the same value as for the PMo_9 ligand ($\varepsilon = 0.75 \times 10^5$ l mol^{-1} cm^{-1}). The ν_1 band, due to dπ–pπ–dπ transitions from the tricentric Mo–O–Mo bonds, is splitted into two shoulders (255 and 280 nm).

Visible and NIR spectra of similar complexes usually show the characteristic d–d transition bands of the coordinated transition metal ion in the octahedral field. However, the expected transition bands cannot be found in the visible spectrum of the PFe_3Mo_9 complex [43]. The very low intensity d–d transitions of the d^5 Fe^{3+} ion, forbidden by the Laporte and spin selection rules, are totally masked by the ν_1 charge transfer band, which extends from UV into the visible range. This indicates that Fe^{3+} ions are also involved in the charge transfer. A single broad band, centred around 850 nm, was recorded in the NIR range and can be assigned to the $^6A_{1g} \rightarrow {}^4T_{1g}(G)$ transition.

3.1.3 EPR spectra

The powder EPR spectrum of the Fe_3PMo_9 complex, recorded at room temperature, exhibits two signals at $g = 4.215$ and 2.004 and also a shoulder at 5.626 (Fig. 1). The spectrum can be interpreted by considering a weak antiferromagnetic coupling between the Fe^{3+} centres of the triangular Fe_3 trinuclear cluster. Simulation of the spectrum was performed by choosing the following parameters: $S = 5/2$ spin state, axial $D = 1.50$ cm^{-1} and rhombic $E = 0.10$ cm^{-1} zero-field splitting.

3.1.4 Magnetic susceptibility

The temperature dependence of the reciprocal molar susceptibility (χ_m^{-1}) of Fe_3PMo_9 complex, in the 77–290 K temperature range, is shown in Fig. 2. Diamagnetic corrections were calculated by using Pascal values. The quasi-linear temperature dependence of the reciprocal molar susceptibility demonstrates a Curie–Weiss behaviour. The calculated effective magnetic moment $\mu_{eff} = 6.06$ μ_B corresponds to a spin state of $S = 5/2$, which is in agreement

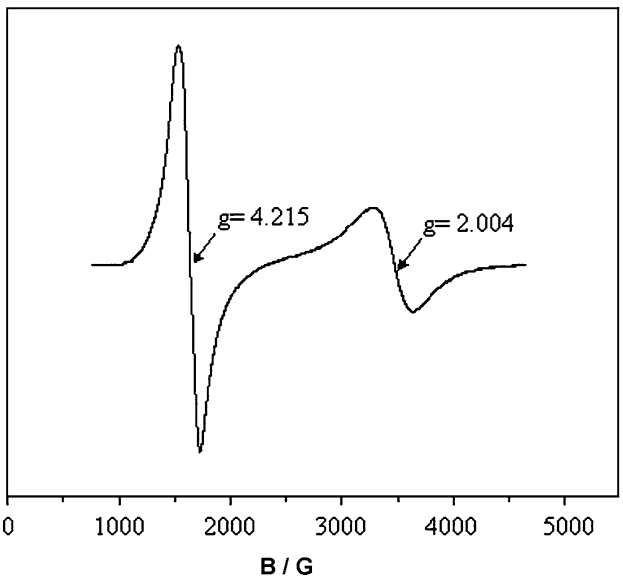

Fig. 1 Powder EPR spectrum of the PFe_3Mo_9 complex recorded in the X band (9.56 GHz), at 293 K. (The *y*-axis indicates the signal intensity in arbitrary units, B is the magnetic field expressed in Gauss, while g is the Landé factor)

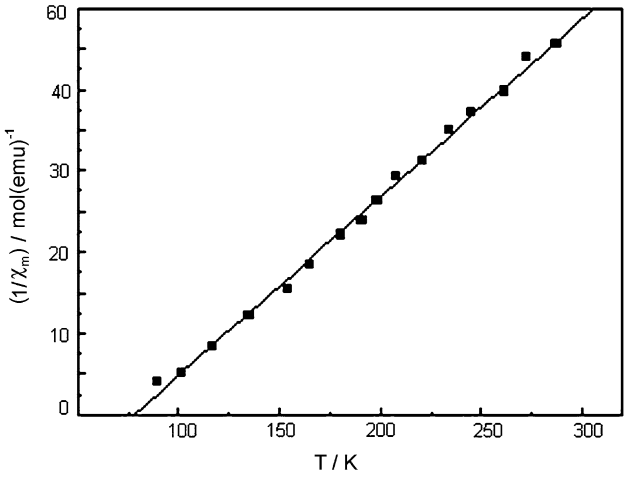

Fig. 2 Temperature dependence of the reciprocal molar susceptibility (χ_m^{-1}) for the PFe_3Mo_9 complex

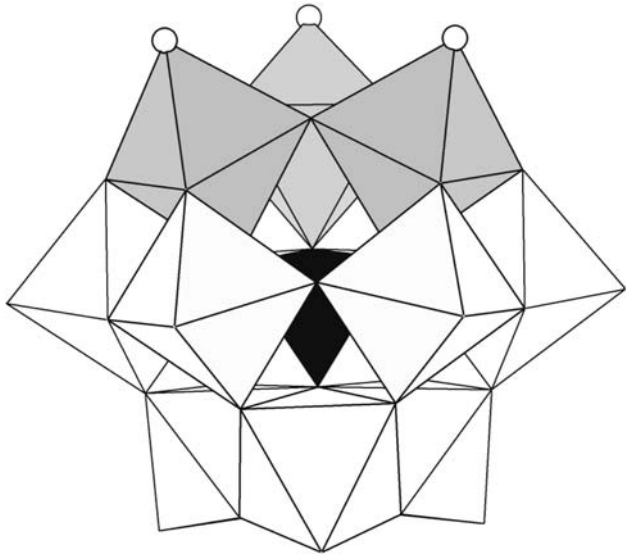

Fig. 3 Polyhedral representation of the reconstituted Keggin-like structure of the Aα-$PFe_3^{III}(H_2O)_3Mo_9^{VI}O_{37}^{6-}$ polyoxometalate anion: (black, PO_4 tetrahedron; white, MoO_6 octahedra; grey, $FeO_5(H_2O)$ octahedra; small circles, H_2O)

with the energy level diagrams obtained from the EPR spectrum. The negative value of the Curie–Weiss temperature ($\theta = -14.3$ K) indicates a weak antiferromagnetic coupling of the three Fe^{3+} metal centres.

3.2 Structure

Unfortunately, the PFe_3Mo_9 complex was obtained as a microcrystalline salt, which did not allow the separation of crystals suitable for X-ray structure analysis. Even so, the investigation results described here strongly support a reconstituted Keggin-like structure for the $A\alpha-PFe_3^{III}(H_2O)_3Mo_9O_{37}^{6-}$ polyoxomolybdate anion, where three Fe^{3+} ions are coordinated as secondary heteroatoms in the sites of the three missing Mo addenda. The positions of the missing terminal O_t atoms in the three corresponding octahedra are occupied by H_2O molecules (Fig. 3). The triangular Fe_3 cluster is formed by edge-sharing $FeO_5(H_2O)$ octahedra. Within the cluster, each $FeO_5(H_2O)$ octahedron contains four oxide ions, a bridging oxygen from the central PO_4 heterogroup and a coordinated H_2O molecule.

3.3 Electrochemical investigation

The electrochemical behaviour of the PFe_3Mo_9 complex was examined in comparison with the PMo_9 ligand, in aqueous acidic solutions (pH 1.5–5.5), where both have good stability [44]. As expected, the voltammetric response of the lacunary PMo_9 ligand (Fig. 4a) reveals three peak pairs, having the formal standard potential values (Table 1) well-placed in the potential domain corresponding to the electrochemical activity of the complete PMo_{12} polyoxometalate. Consequently, the a1/c1–a3/c3 peaks were assigned to the following redox processes [44–46]:

$$\text{a1/c1}\quad PMo_{12}^{VI}O_{40}^{3-} + 2\,e^- + 2\,H^+ \rightarrow H_2PMo_{10}^{VI}Mo_2^{V}O_{40}^{3-} \tag{2}$$

$$\text{a2/c2}\quad H_2PMo_{10}^{VI}Mo_2^{V}O_{40}^{3-} + 2\,e^- + 2\,H^+ \rightarrow H_4PMo_8^{VI}Mo_4^{V}O_{40}^{3-} \tag{3}$$

$$\text{a3/c3}\quad H_4PMo_8^{VI}Mo_4^{V}O_{40}^{3-} + 2\,e^- + 2\,H^+ \rightarrow H_6PMo_6^{VI}Mo_6^{V}O_{40}^{3-} \tag{4}$$

Similarly to the voltammetric response of PMo_9, the cyclic voltammogram of the PFe_3Mo_9 complex (Fig. 4a) shows three pairs of peaks (A1/C1–A3/C3), which are, however, much better shaped and shifted towards more positive potentials (Table 1). It is interesting to note that the formal potential shift observed for the A1/C1 wave (0.194 V) is much higher than that for A3/C3 wave (0.057 V), suggesting that the Fe^{3+} ions of the PFe_3Mo_9 complex exert a stronger influence on the A1/C1 peak pair.

The electrochemical parameters (ΔE_p and I_{pa}/I_{pc}) of the peaks, corresponding to PMo_9 ligand and PFe_3Mo_9 complex (Fig. 4a, Table 1), indicate quasi-reversible redox processes for freely diffusing redox couples [47]. However, the slopes of the log–log dependence between the peak currents and the potential scan rate for the peaks of PFe_3Mo_9 complex (Table 2) reveal that the absorption of the complex on the electrode surface is not negligible (the calculated values of the slopes are significantly higher than 0.5, but lower than 1) [45, 47–49]. All these findings

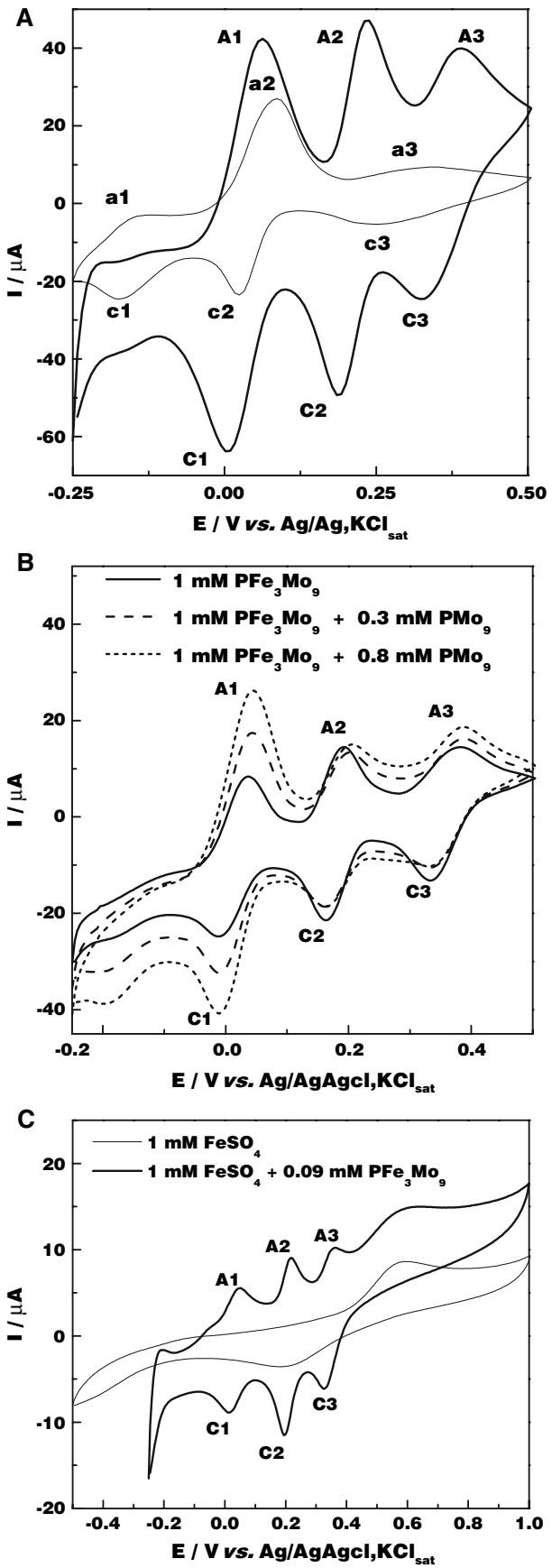

◀ **Fig. 4** Cyclic voltammograms for 10^{-3} M PMo_9 ligand and 10^{-3} M PFe_3Mo_9 complex solutions recorded at graphite electrode (**a**) and the influence of PMo_9 (**b**) and Fe^{2+} (**c**) additions on the PFe_3Mo_9 voltammetric response. Experimental conditions: buffer solution, 0.5 M K_2SO_4 (pH 2.5); potential scan rate, 25 mV s^{-1}; starting potential, −0.25 V versus Ag/AgCl, KCl_{sat}

indicate that the redox processes involved in the electrochemical activity of PFe_3Mo_9 are mixed ones, being both diffusion- and surface-controlled [49, 50].

In order to identify the contribution of the Fe^{3+} ions on the redox response of PFe_3Mo_9 complex, increasing volumes of 1 mM PMo_9 and 1 mM $FeSO_4$ were added to a 1 mM PFe_3Mo_9 solution, and the corresponding cyclic voltammograms were recorded (Fig. 4b and c, respectively). As shown from Fig. 4b, the addition of PMo_9 ligand leds to a significant increase of the A1/C1 peak current, while the other peaks (A2/C2 and A3/C3) remain practically unchanged. Further, the addition of Fe^{2+} ions in the PFe_3Mo_9 ligand solution does not change its voltammetric response (Fig. 4c). However, at a potential value of around +0.6 V versus Ag/AgCl, KCl_{sat}, a new flat peak was observed, which was attributed to the Fe^{2+} oxidation. The effects observed from Fig. 4b and c allow identification of the redox process which generates the A1/C1 peak as identical with that involved in the a1/c1 peak (Eq. 2).

Table 1 Electrochemical parameters of the voltammetric response of PFe_3Mo_9 complex and PMo_9 ligand at graphite electrode

Substance	Peak	ΔE_p/V	$E^{o\prime}$/V versus Ag/AgCl, KCl_{sat}*	I_{pa}/I_{pc}
PMo_9	a1/c1	0.023	−0.162	1.12
	a2/c2	0.061	0.055	1.56
	a3/c3	0.069	0.303	0.46
PFe_3Mo_9	A1/C1	0.046	0.032	1.15
	A2/C2	0.046	0.208	1.01
	A3/C3	0.045	0.360	0.68

Experimental conditions are the same as for Fig. 4

* Standard potential ($E^{o\prime}$) values were calculated as the arithmetic mean of the anodic and cathodic peak potential

Table 2 Influence of the potential scan rate on the voltammetric response of PFe_3Mo_9 complex at graphite electrode

Peak	Slopes of the log (I) versus log (V) dependences		
	Correlation coefficient/No. of experimental points		
	A1/C1	A2/C2	A3/C3
Anodic	0.79	0.76	0.73
	0.995/9	0.997/9	0.989/9
Cathodic	0.82	0.72	0.68
	0.998/9	0.995/9	0.995/7

Experimental conditions are the same as for Fig. 4

Concerning the voltammetric response of the Fe^{3+}/Fe^{2+} redox couple from the PFe_3Mo_9 complex, it should appear at potentials higher than that corresponding to the A1/C1 peak. This statement is supported by the electrochemical behaviour observed for the similar $SiFe^{III}W_{11}$ complex [51, 52], where the peak attributed to the Fe^{3+}/Fe^{2+} couple is placed at a more positive potential than those corresponding to the SiW_{11} ligand [51, 52].

The PMo_9 ligand is stable in acidic media [44, 49, 53, 54]. This behaviour was also confirmed for the PFe_3Mo_9 complex. Thus, for all observed peaks (A1/C1–A3/C3), the plots I_p versus pH show that the peak current of the PFe_3Mo_9 complex presents a maximum at pH ~2.5 (results not shown). Furthermore, as expected, the cyclic voltammograms recorded for the PFe_3Mo_9 complex in acidic media are gradually shifted towards more positive potentials with the pH decrease [47, 49, 53]. As Fig. 5a reveals, the formal standard potentials ($E^{o\prime}$) of the A1/C1–A3/C3 peaks depend linearly on the pH of the supporting electrolyte. The slopes of these curves are listed in Table 3, and indicate that the H^+/electron ratios involved in the redox processes that generate the A1/C1 and A2/C2 peaks are close to 1, while for the A3/C3 peak the respective ratio is close to 0.5. This behaviour corroborates the above results, confirming that for peak pairs A1/C1 and A2/C2, $2H^+$ and $2e^-$ are exchanged (Eqs. 5, 6). By considering that the Fe^{3+}/Fe^{2+} redox couple, incorporated in the structure of PFe_3Mo_9, is relatively insensitive to pH changes [47], and the experimental evidence showing that H^+ and $2e^-$ are involved in the process that accounts for the A3/C3 peak, one can assume that the A3/C3 peak is generated by an overlap of Fe^{3+}/Fe^{2+} and the oxocage voltammetric responses (Eq. 7). From Fig. 5b it is seen that for the A3/C3 peak, the pH dependence of the formal standard potential remains unchanged, irrespective of the potential scan rate used to record the PFe_3Mo_9 voltammetric response.

Consequently, the following charge transfers and equations are proposed for A1/C1–A3/C3 peaks:

$$\text{A1/C1}\quad PFe_3^{III}(H_2O)_3Mo_9^{VI}O_{37}^{6-} + 2H^+ + 2e^- \rightarrow H_2PFe_3^{III}(H_2O)_3Mo_7^{VI}Mo_2^{V}O_{37}^{6-} \tag{5}$$

$$\text{A2/C2}\quad H_2PFe_3^{III}(H_2O)_3Mo_7^{VI}Mo_2^{V}O_{37}^{6-} + 2H^+ + 2e^- \rightarrow H_4PFe_3^{III}(H_2O)_3Mo_5^{VI}Mo_4^{V}O_{37}^{6-} \tag{6}$$

$$\text{A3/C3}\quad H_4PFe_3^{III}(H_2O)_3Mo_5^{VI}Mo_4^{V}O_{37}^{6-} + H^+ + 2e^- \rightarrow H_5PFe^{III}Fe_2^{II}(H_2O)_3Mo_5^{VI}Mo_4^{V}O_{37}^{7-} \tag{7}$$

The mediated electroreduction of H_2O_2 is of general interest for many practical applications, such as biosensors and fuel cells [47, 55]. While H_2O_2 reduction on conventional electrodes requires large overpotentials [50, 53], it was reported that the electroreduction of H_2O_2 can be activated by

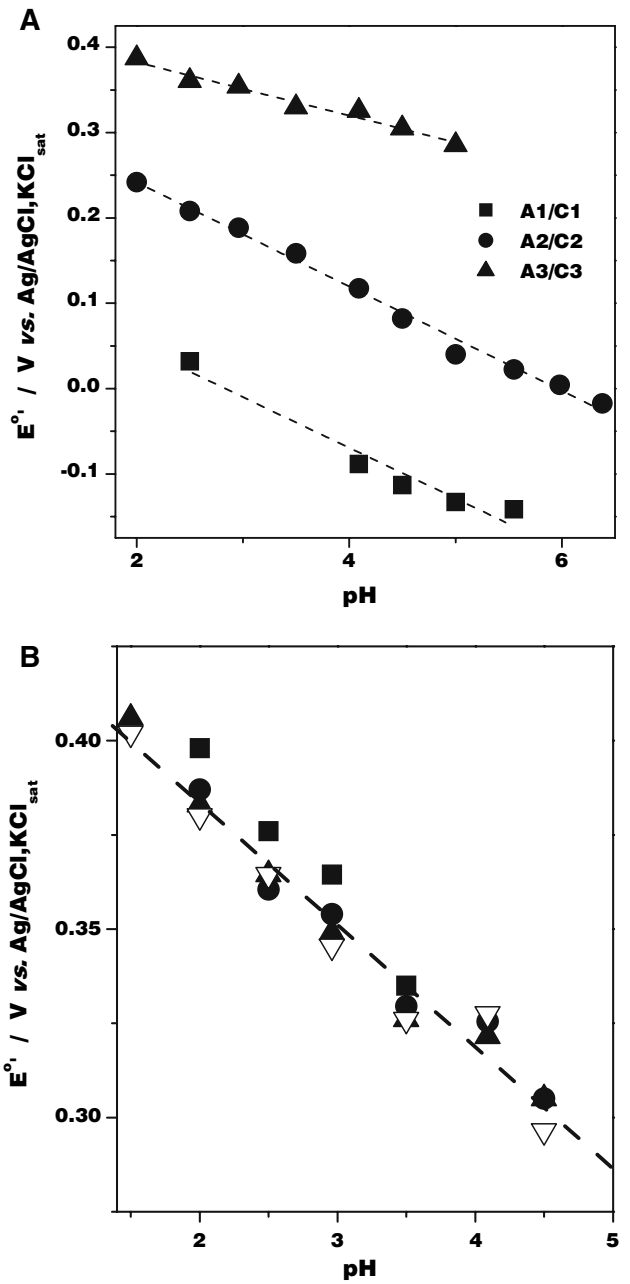

Fig. 5 pH dependence of formal standard potentials of redox couples involved in the voltammetric response of PFe_3Mo_9 complex, at 25 mV s^{-1} (**a**) and, in the case of A3/C3 peak, recorded at several potential scan rates: 5 mV s^{-1} (■), 25 mV s^{-1} (●), 50 mV s^{-1} (▲), 100 mV s^{-1} (▽) (**b**). The rest of the experimental parameters are the same as for Fig. 4

phosphopolyoxomolybdates [55]. Being readily reduced at quite positive potentials these complexes serve as powerful electron pumps [55]. In order to verify whether the presence of Fe^{3+} ions exerts a noticeable effect on this reaction, the electrocatalytic activity of PFe_3Mo_9 complex in the H_2O_2 electroreduction was investigated in comparison with PMo_9 (Fig. 6). Enhanced catalytic reduction of H_2O_2 on graphite,

Table 3 Estimation of the proton/electron (p/n) ratio corresponding to the redox couples involved in the voltammetric response of 10^{-3} M PFe_3Mo_9 complex

Parameters	A1/C1	A2/C2	A3/C3
Slope*	0.0594	0.0610	0.0310
R/No. of points	0.975/5	0.985/10	0.987/7
p/n	1.01	1.03	0.52

Experimental conditions are the same as for Fig. 5a

* Slope corresponds to the pH dependence of the formal standard potential of Fe_3PMo_9 complex

due to the presence of PFe_3Mo_9 complex dissolved in the supporting electrolyte, is shown by Fig. 6. The A1/C1 peak pair is the most sensitive to H_2O_2 addition. For this reason and because of the relatively low value of its formal standard potential (well-placed in the optimal domain for amperometric detection of H_2O_2 [56]) the A1/C1 peak pair was selected for exploiting the electrocatalytic activity of PFe_3Mo_9 complex.

Cyclic voltammograms, performed after successive additions of H_2O_2, yield the calibration curve for H_2O_2 detection (see inset in Fig. 6). Supposing that the investigated system follows a Michaelis–Menten kinetics, the corresponding kinetic parameters were estimated as follows: $K_M = 1.92 \pm 0.11$ mM and $I_{max} = 1.94 \pm 0.46$ μA ($R^2 = 0.99749$, n = 7). The catalytic efficiency [calculated as CE (%) $= \Delta I_{pc}/I_{pc,0}$, where $\Delta I_{pc} = (I_{pc,H_2O_2} - I_{pc,0})$, I_{pc,H_2O_2} and $I_{pc,0}$ are the cathodic peak currents recorded for A1/C1 wave, in the presence and absence of H_2O_2, respectively] was found to be 12.7% for 1 mM H_2O_2 (10 mM PFe_3Mo_9).

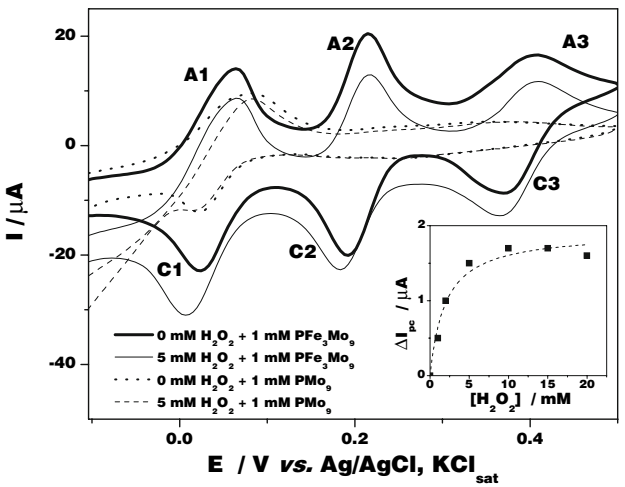

Fig. 6 Electrocatalytic activity of PFe_3Mo_9 complex for H_2O_2 reduction. Inset: dependence on the H_2O_2 concentration of the corrected cathodic peak current $\Delta I_{pc} = (I_{pc,H_2O_2} - I_{pc,0})$ for A1/C1 wave. Experimental conditions: applied electrode potential, −0.1 V versus Ag/AgCl/ KCl_{sat}; the rest of experimental parameters are the same as for Fig. 4

The calculated sensitivity, estimated as the ratio $I_{max}/K_M = 1.01$ mA M^{-1}, was found to be much greater than the corresponding value for the Dawson P_2Mo_{18} polyoxometalate (2.27 μA M^{-1} [56]). This demonstrates that the higher sensitivity, observed for H_2O_2 electroreduction in the presence of PFe_3Mo_9 complex, is probably due to the presence of Fe^{3+} ions/metal centres.

4 Conclusions

A new triiron complex of the Keggin trilacunary PMo_9 polyoxomolybdate, i.e. PFe_3Mo_9, was synthesized and characterized by elemental analysis, FTIR, Raman, UV-VIS-NIR and EPR spectroscopy, and also by magnetic susceptibility measurements.

CV performed under different experimental conditions (various scan rates, pH and composition of the supporting electrolyte) was used for investigating the electrochemical behaviour of PFe_3Mo_9 complex in acidic medium. The results allow identification of the redox processes responsible for the voltammetric response of the PFe_3Mo_9 complex. At the same time it has been demonstrated that, due to the presence of the Fe^{3+} ions, the new complex is able to catalyse the electroreduction of H_2O_2 with higher efficiency as compared to the PMo_9 ligand.

Acknowledgements Part of this work was supported by the research grant A-34/1529/2007 from the National University Research Council.

References

1. Pope MT, Müller A (1994) Polyoxometalates: from platonic solids to anti-retroviral activity. Kluwer, Dordrecht
2. Pope MT, Müller A (2001) Polyoxometalate chemistry: from topology via self-assembly to applications. Kluwer, Dordrecht
3. Müller A, Luban A, Schröder M et al (2001) ChemPhysChem (Concepts) 2:517
4. Yamase T, Pope MT (2002) Polyoxometalate chemistry for nano-composite design. Kluwer, New York
5. Müller A (2003) Science 300:749
6. Patrut A (2005) In: Diudea M (ed) Nanostructures: novel architecture. Nova Science, New York, pp 361–397
7. Müller A, Roy S (2005) Eur J Inorg Chem 3561
8. Pope MT (1983) Heteropoly and isopoly oxometalates. Springer, Berlin
9. Baker LCW, Glick DC (1998) Chem Rev 98:3
10. Müller A, Peters F, Pope MT, Gatteschi D (1998) Chem Rev 98:239
11. Day W, Klemperer WG (1985) Science 233:533
12. Klemperer WG, Yagasaki A (1989) Chem Lett 2041
13. Liu J, Ortega F, Sethuraman P et al (1992) J Chem Soc Dalton Trans 1901
14. Lyon DK, Miller WK, Novet T et al (1991) J Am Chem Soc 113:7209
15. Katsoulis DE, Pope MT (1989) J Chem Soc Dalton Trans 1483

16. Neumann JR, Abu-Gnim C (1990) J Am Chem Soc 112:6025
17. Song WB, Wang XH, Liu Y et al (1999) J Electroanal Chem 476:85
18. Mizuno N, Misono M (1998) Chem Rev 98:199
19. Sadakane M, Steckhan E (1998) Chem Rev 98:219
20. Zonnevijlle F, Tourné CM, Tourné GF (1982) Inorg Chem 21:2751
21. Toth JE, Anson FC (1988) J Electroanal Chem 256:361
22. Toth JE, Anson FC (1989) J Am Chem Soc 111:2444
23. Toth JE, Melton JD, Cabelli D et al (1990) Inorg Chem 29:1952
24. Finke RG, Lyon DK, Nomiya K et al (1990) Inorg Chem 29:1784
25. Dong S, Liu M (1994) J Electroanal Chem 372:95
26. Zhang XQ, Chen Q, Duncan DC et al (1997) Inorg Chem 36:4208
27. Zhang XQ, Chen Q, Duncan DC et al (1997) Inorg Chem 36:4381
28. Mizuno N, Nozaki C, Kiyoto I, Misono M (1998) J Am Chem Soc 120:9267
29. Nozaki C, Kiyoto I, Minai Y et al (1999) Inorg Chem 38:5724
30. Gaspar S, Muresan L, Patrut A, Popescu IC (1999) Anal Chim Acta 395:111
31. Mizuno N, Nishiyama Y, Kiyoto I, Misono M (2000) Stud Surf Sci Catal 130:797
32. Knap C, Ui T, Nagai K, Mizuno M (2001) Catal Today 71:111
33. Min JS, Misono M, Taguchi A, Mizuno M (2001) Chem Lett 28
34. Ruhlmann L, Canny J, Contant R, Thouvenot R (2002) Eur J Inorg Chem 975
35. Liu J, Cheng S, Dong S (2002) Electroanalysis 14:569
36. Bi L, Liu J, Shen Y et al (2003) New J Chem 27:756
37. Zhai S, Gong S, Jiang J et al (2003) Anal Chim Acta 486:85
38. Etienne E, Cavani F, Mezzogori R et al (2003) Appl Catal A Gen 256:275
39. Mizuno N, Min JS, Taguchi A (2004) Chem Mater 16:2819
40. Massart R, Contant R, Fruchart J-M et al (1977) Inorg Chem 16:2916
41. Rocchiccioli-Deltcheff C, Thouvenot R, Franck R (1976) Spectrochim Acta 32A:587
42. So H, Pope MT (1972) Inorg Chem 11:1441
43. Lever BP (1984) Inorganic electronic spectroscopy. Elsevier, New York
44. Sadakane M, Steckhan E (1998) Chem Rev 98:219
45. Li Z, Chen J, Pan D, Tao W, Nie L, Yao S (2006) Electrochim Acta 51:4255
46. Martel D, Gross M (2007) J Solid State Electrochem 11:421
47. Bi L, Liu J, Shen Y, Junguang J, Dong S (2003) New J Chem 27:756
48. Liu H, He P, Li Z, Sun C, Shi L, Liu Y, Zhu G, Li J (2005) Electrochem Commun 7:1357
49. Zou X, Shen Y, Peng Z, Zhang L, Bi L, Wang Y, Dong S (2004) J Electroanal Chem 566:63
50. Han Z et al (2005) J Solid State Chem 178:1386
51. Song W, Wang X, Liu Y, Liu J, Xu H (1999) J Electroanal Chem 476:85
52. Toth JE, Melton J D, Cabelli D, Bielski BHJ, Anson FC (1990) Inorg Chem 29:1952
53. Wang X, Zhang H, Wang E, Han Z, Hu C (2004) Mater Lett 58:1661
54. Keita B, Girard F, Nadjo L, Contant R, Belghiche R, Abbessi M (2001) J Electroanal Chem 508:70
55. Martel D, Kuhn A (2000) Electrochim Acta 45:1829
56. Gorton L (1995) Electroanalysis 7:23